12th International Symposium on Turbulence and Shear Flow Phenomena (TSFP12)
Osaka, Japan (Online), July 19-22, 2022

EFFECTS OF INITIAL CONDITIONS ON MIXING IN WALL-BOUNDED TURBULENT FLOW

Milind Singh
Department of Mechanical Engineering
McGill University
Montréal, Canada
milind.singh2@mail.mcgill.ca

Emmanuel Germaine
Department of Mechanical Engineering
McGill University
Montréal, Canada
emmanuel.germaine@mail.mcgill.ca

Laurent Mydlarski
Department of Mechanical Engineering
McGill University
Montréal, Canada
laurent.mydlarski@mcgill.ca

Luca Cortelezzi
Department of Aerospace Science and Technology
Politecnico di Milano
Milano, Italy
luca.cortelezzi@polimi.it

ABSTRACT

Scalar mixing occurs in a wide variety of environmental and engineering flows. Given that the majority of these flows are turbulent, a more complete understanding of the mechanisms that underlie the scalar mixing process is required to predict and control these flows and the evolution of the concentration(s) of the scalar(s) therein. Direct numerical simulations (DNSs) are particularly useful in the study of turbulence since DNSs resolve the full range of (length and time) scales in turbulent flows. The present work employs a spectral approach for simulating the hydrodynamic field, and a flux integral method for computing the advection and diffusion of the passive scalar. Mixing of the latter is studied in a fully developed turbulent channel flow, and particular attention is paid to the evolution of the scalar dissipation rate and the differences that arise from different scalar-field initial conditions. Observed differences in the evolutions for the three initial conditions investigated are explained by an analysis of the different terms that comprise the scalar disspation rate budget. To promote mixing in a wall-bounded flow, it is recommended that scalar interfaces be aligned normal to the mean velocity vector, to enhance the stretching of the interface.

INTRODUCTION

Scalar quantities (e.g. temperature, humidity, chemical species concentration) are mixed within a wide range of environmental and engineering flows (e.g. the atmosphere, which transports temperature and humidity; the oceanic mixed layer, in which temperature and salinity are mixed; chemical reactors; heat exchangers, combustion processes, etc.). Given that the vast majority of these flows are turbulent, an understanding of the turbulent scalar mixing process is required to predict (and, ultimately, control) these flows and the evolution of the concentration(s) of the scalar(s) therein. Thus, the present work investigates the turbulent mixing of (passive) scalars, which are governed by the advection-diffusion equation:

$$\frac{\partial \tilde{\theta}}{\partial t} + \tilde{u}_j \frac{\partial \tilde{\theta}}{\partial x_j} = \alpha \frac{\partial^2 \tilde{\theta}}{\partial x_j \partial x_j} \tag{1}$$

where $\tilde{\theta}$ represents the instantaneous scalar field, $\tilde{u}_j$, $j = 1,2,3$ are the components of the instantaneous velocity vector field, α is the scalar's molecular diffusivity within the fluid, and repeated indices imply Einstein's summation convention.

The present work focusses on the mixing of scalars within a fully-developed, high-aspect-ratio turbulent channel flow, to model the behavior of real flows and the physical processes therein (as opposed to studying mixing within homogeneous flows). Channel flow is especially appropriate because it is the simplest realization of an inhomogeneous turbulent flow.

Mixing metrics are often used to quantify the efficacy of a scalar mixing process. These include i) the unmixedness parameter (Danckwerts, 1952; Dimotakis & Miller, 1990):

$$\Xi \equiv \frac{\langle \theta^2 \rangle}{\Theta(1-\Theta)}; \;\; 0 \leq \Xi \leq 1 \tag{2}$$

where Θ is the average scalar concentration, θ is its fluctuation, and angular brackets denote averages, or ii) a multi-scale norm, such as the mix-norm (Mathew *et al.*, 2005):

$$\mu_\theta = \left[\sum_{k \in Z^3} \frac{1}{\sqrt{1+4\pi^2||\mathbf{k}^2||}} |\hat{\Theta}_k(t)|^2 \right]^{1/2} \tag{3}$$

where $\mathbf{k}$ is the wavevector, and $\hat{\Theta}_k$ are the Fourier coefficients of a spectral representation of the scalar field. Note that the two metrics are very different: the unmixedness quantifies molecular mixing only, whereas the mix-norm quantifies mixing by accounting for both stirring and molecular mixing. These differences have a notable impact on the results using these metrics. For example, consider the idealized case of mixing in two dimensions of two hypothetical fluids (one white and one black, and both having molecular diffusivities equal to zero). Let one then assume that the fluid could be stirred in such a way that the end result would be a configuration similar to a chessboard, with white and black squares at the smallest scales. In this case, the unmixedness would be maximum (because there is no molecular mixing) whereas the mix-norm will be minimum, because the stirring is complete.

Motivation for the present study stems from observations by Gubanov & Cortelezzi (2009) and Germaine *et al.* (2018),

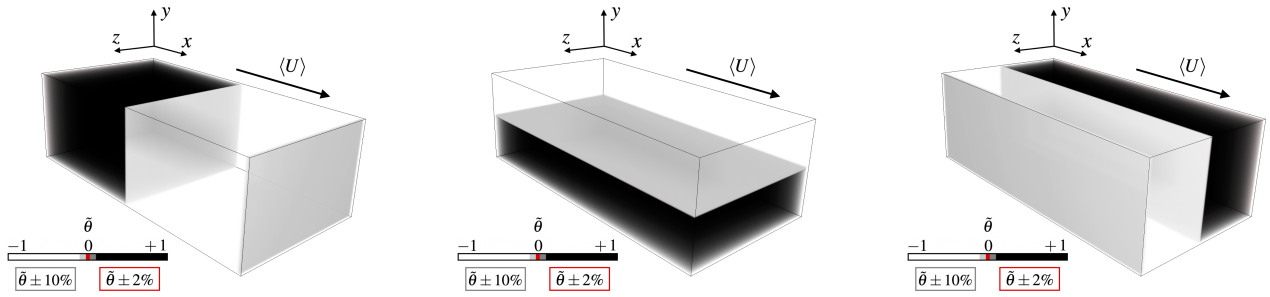

(a) IC_x (b) IC_y (c) IC_z

Figure 1: The three scalar-field initial conditions studied herein. Imagery generated using VAPOR (Li *et al.*, 2019).

who have observed that scalar fields, including the evolution of the scalar dissipation rate, are strongly affected by the initial conditions of the scalar field, even when these initial conditions are mixed by identical hydrodynamic fields. It is therefore of interest to investigate the nature of the physical processes that lead to such different evolutions of the scalar field.

The objective of the present work is therefore to investigate the effect of scalar-field initial conditions on mixing that occurs within fully developed, turbulent channel flow. This will be undertaken by way of an initial comparison between the evolutions of the two aforementioned mixing metrics and the scalar dissipation rate in turbulent flows. However, the primary focus of the present work will be an investigation of the evolution of the scalar fields for the different initial conditions, by way of an analysis of the various terms in the evolution equation (i.e. budget) of the scalar dissipation rate: ($\varepsilon_\theta \equiv \alpha \frac{\partial \theta}{\partial x_j}\frac{\partial \theta}{\partial x_j}$):

$$\begin{aligned}\frac{\partial \langle \varepsilon_\theta \rangle}{\partial t} + U_j \frac{\partial \langle \varepsilon_\theta \rangle}{\partial x_j} = &-2\alpha \frac{\partial U_j}{\partial x_i}\langle \frac{\partial \theta}{\partial x_i}\frac{\partial \theta}{\partial x_j}\rangle - 2\alpha \frac{\partial \Theta}{\partial x_j}\langle \frac{\partial u_j}{\partial x_i}\frac{\partial \theta}{\partial x_i}\rangle \\ &-2\alpha \langle u_j \frac{\partial \theta}{\partial x_i}\rangle \frac{\partial^2 \Theta}{\partial x_i \partial x_j} - 2\alpha \langle \frac{\partial u_j}{\partial x_i}\frac{\partial \theta}{\partial x_i}\frac{\partial \theta}{\partial x_j}\rangle \\ &+ \frac{\partial}{\partial x_j}\left(\alpha \frac{\partial \langle \varepsilon_\theta \rangle}{\partial x_j} - \langle u_j \varepsilon_\theta \rangle\right) \\ &-2\alpha^2 \langle \frac{\partial^2 \theta}{\partial x_i \partial x_j}\frac{\partial^2 \theta}{\partial x_i \partial x_j}\rangle \end{aligned} \quad (4)$$

where U_j is the mean velocity vector, and u_j is the velocity fluctuation.

SIMULATIONS

The investigations herein employ numerical simulations of both the turbulent velocity and passive scalar fields, in which the latter is advected by the former. The turbulent velocity field is calculated via direct numerical simulation (DNS), which resolves all scales of the flow by solving the Navier-Stokes equations with constant properties. The DNS of the velocity field is computed using a code entitled CHANNELFLOW (Gibson *et al.*, 2008; Gibson, 2010; http://channelflow.org/) which uses spectral discretization in space (Fourier × Chebyshev × Fourier), and a third-order semi-implicit backwards differentiation scheme in time, with no-penetration / no-slip boundary conditions imposed at the walls of the channel ($y = 0$ and $y = 2h$, where h is the half-height of the channel), and periodic boundary conditions in the streamwise (x) and spanwise (z) directions. Simulation of the hydrodynamic field is conducted at $Re_\tau = 190$ over a domain of size $2\pi h \times 2h \times \pi h$, in the streamwise ($x$), wall-normal ($y$) and spanwise ($z$) directions, respectively, with a resolution of $256 \times 193 \times 192$. ($Re_\tau \equiv u_\tau h/\nu$, $u_\tau \equiv \sqrt{\nu \times \partial U/\partial y|_{y=0}}$, and ν is the kinematic viscosity of the fluid.) The resulting turbulent velocity field is statistically steady and statistically one-dimensional, such that $\langle U \rangle = \langle U \rangle(y)$ only.

The pre-computed velocity field is used as an input to the advection-diffusion solver, and is interpolated from a spectral to a finite-volume representation via spectral (exact) interpolation. A very small correction is applied to the streamwise component of the velocity field to ensure the exact divergence-free condition. The advection-diffusion equation is solved using a fully three-dimensional and cost-effective flux integral method entitled 3DFLUX (Germaine *et al.*, 2013). The fully explicit and multidimensional nature of the approach ensures that it is free of splitting errors, and provides a better convergence rate of the numerical errors when compared to commonly used one-dimensional methods. A semi-Lagrangian approach is implemented in 3DFLUX by discretizing the spatial domain on an Eulerian grid and using a Lagrangian frame of reference for temporal discretization. Solutions for the advection-diffusion equation are obtained using non-overlapping control volumes to discretize the computational domain and estimate the flux exchanged between adjacent cells. DNS of the scalar field is undertaken on the same domain of $2\pi h \times 2h \times \pi h$, with a resolution of $514 \times 195 \times 194$ to resolve both the large and small scales of the scalar field. It is assumed that the magnitudes of the scalar fluctuations are sufficiently small, such that the dynamics of the velocity field are independent from the scalar field and the scalar is considered as being passive.

As noted above, the evolution of the mixing with time will be studied for three different scalar-field initial conditions, IC_x, IC_y and IC_z, as depicted in figure 1. These fields consist of two equal volumes of uniform concentrations, $\tilde{\theta} = +1$ (black) and -1 (white), separated by two interfaces (due to the periodic boundary conditions in x and z) of total area $4\pi h^2$ ($= 2 \times 2h \times \pi h$) for IC_x and $8\pi h^2$ ($= 2 \times 2h \times 2\pi h$) for ICz and a single interface of area $2\pi^2 h^2$ ($= 2\pi h \times \pi h$) for ICy. All fields have zero mean concentration. Note that all three scalar fields are subjected to identical turbulent velocity fields, and thus any differences in the evolutions of the three scalar fields are the sole result of the orientations of the interfaces defining the initial scalar fields relative to that of the velocity field.

RESULTS

Inspired by the results of Germaine *et al.* (2018), who investigated the dependence of local anisotropy of passive scalars on their initial conditions, we plot in figure 2 the scalar field distributions that result from the action of the identical turbulent channel flow (velocity field) on scalar fields subjected to the three aforementioned, distinct initial conditions

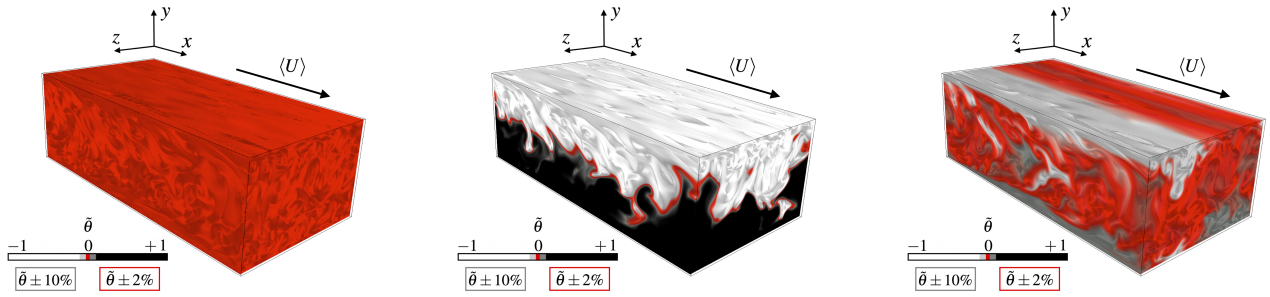

(a) IC_x (b) IC_y (c) IC_z

Figure 2: Concentration distributions generated at $\tau = 7$ by the action of the same turbulent channel flow on the three scalar-field initial conditions. Imagery generated using VAPOR (Li *et al.*, 2019).

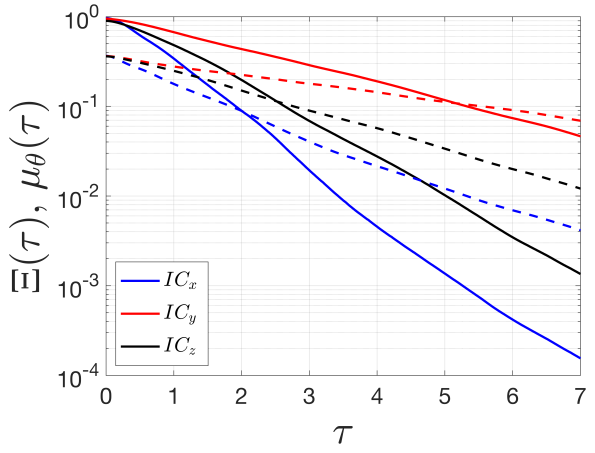

Figure 3: Time-evolution of the unmixedness parameter (solid line) and the mix-norm (dashed line) for the scalar fields resulting from the three initial conditions.

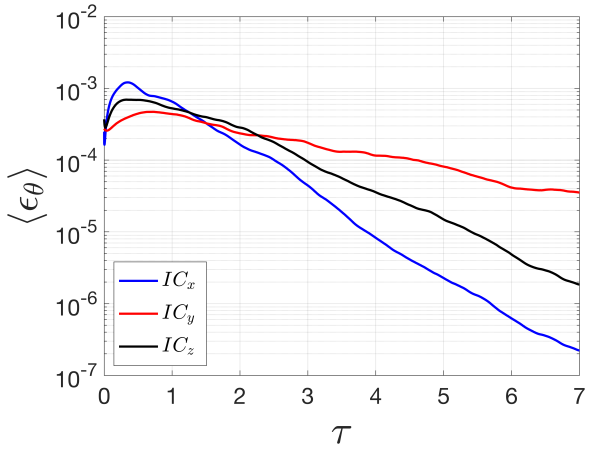

Figure 4: Time-evolution of the volume-averaged (i.e. $\langle\cdot\rangle = \langle\cdot\rangle_{x,y,z}$) scalar dissipation rates for the scalar fields resulting from the three initial conditions.

for a period of $\tau(\equiv tu_\tau/h) = 7$. From this figure, it is readily observed that the scalar field resulting from the IC_x initial condition is the best mixed, whereas that resulting from the IC_y initial condition is the least well mixed. This is already an intriguing result and indicates that the initial conditions can strongly influence the subsequent mixing. Moreover, it is worth reiterating that all three scalar-field initial conditions were comprised of equal parts "black fluid" (i.e. scalar with an initial concentration $\tilde{\theta} = +1$) and "white fluid" (i.e. scalar with an initial concentration $\tilde{\theta} = -1$). Thus the rate at which mixing will occur in such an inhomogeneous flow (as is the flow in all real devices) is highly dependent on the initial configuration of the two quantities being mixed.

To quantify the mixing, we plot the time-evolutions of the unmixedness parameter (Ξ) and the mix-norm (μ_θ) for the three scalar-field initial conditions in figure 3. One observes that the unmixedness starts very close to its maximum value of 1, whereas the initial values for the mix-norm fall between 0.3 and 0.4 (because the latter depend on the initial geometry of the scalar field). However, shortly after the velocity field starts mixing the scalar field, the time-evolutions for both mixing metrics follow a similar pattern; i.e. the evolutions of both Ξ and μ_θ decay exponentially with time, with the most efficient stirring and mixing (i.e. fastest rates of decay of Ξ and μ_θ) occurring for the IC_x case and the slowest for the IC_y case.

Given the objective of attempting to tie the evolutions of the mixing metrics to the underlying physics of the turbulence, we first plot the evolutions of the (volume-averaged) scalar dissipation rates ($\langle\varepsilon_\theta\rangle$) corresponding to the fields with the three initial conditions as a function of time in figure 4. Although some differences exist at early times ($\tau < 1$), the long term evolution of $\langle\varepsilon_\theta\rangle$ is qualitatively similar to the evolutions of both Ξ and μ_θ – the dissipation rates decrease at rates dependent upon the initial conditions of the scalar field, with the the fastest decrease in $\langle\varepsilon_\theta\rangle$ occurring for IC_x, corresponding to the most efficient mixing, and the slowest corresponding to IC_y. At shorter times, $\langle\varepsilon_\theta\rangle$ increases, presumably due to the stretching and stirring of the interface between the two (i.e. the "black" and "white") scalar fields, which results in a production of $\langle\varepsilon_\theta\rangle$. This is in contrast with the short-time evolutions of both Ξ and μ_θ, which are both monotonically decreasing functions of time for all values of τ. Note that the values of $\langle\varepsilon_\theta\rangle$ for the IC_x and IC_z cases peak around $\tau \approx 1/3$, whereas the peak in $\langle\varepsilon_\theta\rangle$ for the IC_y case occurs later, around $\tau \approx 2/3$.

Before proceeding, we are obliged to discuss the issue of averaging when presenting the results for the individual terms in eq. (4). In particular, the homogeneity (or lack thereof) of both the velocity and scalar fields in this work must be considered in the analysis of the results. Whereas the velocity field is statistically homogeneous in the x- and z-directions, as well as being statistically stationary, the natures of the scalar fields resulting from the action of the velocity field on the three different initial conditions are all different. The scalar field resulting from the IC_x initial condition is statistically homogeneous in the z-direction (only). That resulting from the IC_y initial condition is statistically homogeneous in the x- and z-directions. Lastly, the scalar field resulting from the IC_z ini-

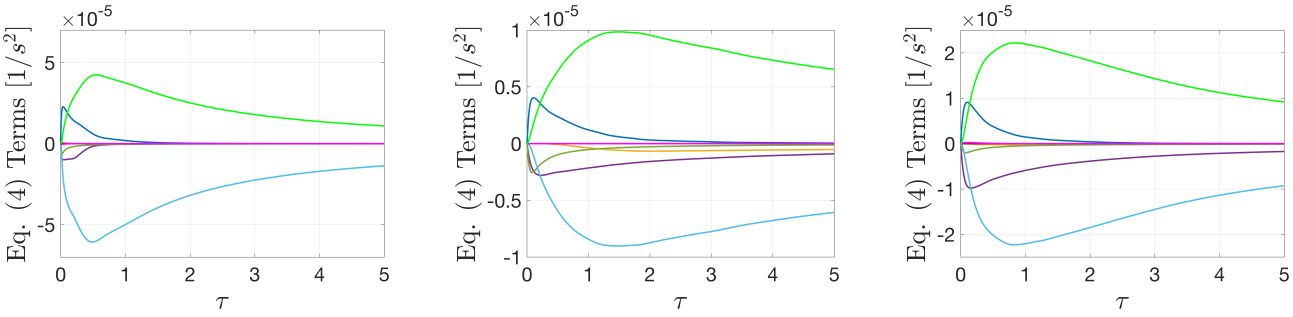

(a) IC_x (b) IC_y (c) IC_z

Figure 5: Evolution in time of the space- and time-averages of all 9 terms in the scalar dissipation rate budget in which statistical moments ($\langle\cdot\rangle$) are assessed in planes parallel to the initial location of the interface in the initial condition. (a) IC_x with $\frac{1}{L_x}\frac{1}{\tau}\int_0^{L_x}\int_0^{\tau} Term\, d\tau'\, dx$, (b) IC_y with $\frac{1}{2h}\frac{1}{\tau}\int_0^{2h}\int_0^{\tau} Term\, d\tau'\, dy$, and (c) IC_z with $\frac{1}{L_z}\frac{1}{\tau}\int_0^{L_z}\int_0^{\tau} Term\, d\tau'\, dz$.

Table 1: Legend for the various terms in the budget of the scalar dissipation rate.

Color	Term #	Term	Physical interpretation
	(i)	$\frac{\partial}{\partial t}\langle\varepsilon_\theta\rangle$	time rate of change of $\langle\varepsilon_\theta\rangle$
	(ii)	$\langle U_j\rangle\frac{\partial}{\partial x_j}\langle\varepsilon_\theta\rangle$	mean flow advection of $\langle\varepsilon_\theta\rangle$
	(iii)	$2\alpha\frac{\partial\langle U_j\rangle}{\partial x_i}\langle\frac{\partial\theta}{\partial x_i}\frac{\partial\theta}{\partial x_j}\rangle$	production of $\langle\varepsilon_\theta\rangle$ by mean velocity gradients
	(iv)	$2\alpha\frac{\partial\langle\Theta\rangle}{\partial x_j}\langle\frac{\partial u_j}{\partial x_i}\frac{\partial\theta}{\partial x_i}\rangle$	production of $\langle\varepsilon_\theta\rangle$ by mean scalar gradients
	(v)	$2\alpha\frac{\partial^2\langle\Theta\rangle}{\partial x_i\partial x_j}\langle u_j\frac{\partial\theta}{\partial x_i}\rangle$	mixed production of $\langle\varepsilon_\theta\rangle$
	(vi)	$2\alpha\langle\frac{\partial u_j}{\partial x_i}\frac{\partial\theta}{\partial x_i}\frac{\partial\theta}{\partial x_j}\rangle$	production of $\langle\varepsilon_\theta\rangle$ by turbulent vortex stretching
	(vii)	$-\alpha\frac{\partial^2}{\partial x_j\partial x_j}\langle\varepsilon_\theta\rangle$	molecular transport of $\langle\varepsilon_\theta\rangle$
	(viii)	$\frac{\partial}{\partial x_j}\langle u_j\varepsilon_\theta\rangle$	turbulent advection of $\langle\varepsilon_\theta\rangle$
	(ix)	$2\alpha^2\langle\frac{\partial^2\theta}{\partial x_i\partial x_j}\frac{\partial^2\theta}{\partial x_i\partial x_j}\rangle$	molecular dissipation of $\langle\varepsilon_\theta\rangle$

tial condition is statistically homogeneous in the x-direction (only). Moreover, all scalar-field statistics studied in this work are non-stationary, due to the evolution in time of the scalar fields from the unmixed to the mixed states. Thus the underlying symmetries and ensuing statistical homogeneities associated with the different initial conditions, as well as the statistically non-stationary nature of the scalar field, must be taken into account when analyzing the results. A specific consequence is that one can no longer volume-average the terms in eq. (4) if one wants to examine the evolution of all its nine constituent terms, because all but three of them (the first, sixth and ninth), will be zero when volume-averaged. Secondly, there is no "universal" approach to spatial averaging that can be employed in this analysis that will not eliminate some of the nine terms in eq. (4) in some of the scalar fields. For example, were one to average scalar-field statistics in the z-direction, certain terms in the $\langle\varepsilon_\theta\rangle$ budget (such as production by the mean scalar gradient) will become zero for the IC_z case, only, because $\partial\langle\cdot\rangle_z/\partial z = 0$ (by definition). Lastly, given that volume-averaging is no longer feasible and we will therefore employ averages taken over (spatial) planes (at specific locations within the channel) to investigate the terms in eq. (4), the statistical convergence of the data is reduced, given that averages will be taken over less data. To address this, local time averages will be employed (i.e. averaging the value of a term in the budget of $\langle\varepsilon_\theta\rangle$ from $\tau' = 0$ to $\tau' = \tau$), which will improve convergence of the data, while retaining its time-dependence. Moreover, figure 5 will also calculate local spatial averages after having performed the time-average, which, when calculated in this way, does not eliminate terms and further aids convergence.

Having discussed the issue of averaging, we plot in figure 5 the contributions of the terms in the budget of $\langle\varepsilon_\theta\rangle$ (eq. (4)) to further investigate the evolutions of $\langle\varepsilon_\theta\rangle$ depicted in figure 4. (A legend corresponding to the 9 terms of eq. (4) is given in table 1.) Multiple observations can be made from the plots therein to provide insight into the evolutions of $\langle\varepsilon_\theta\rangle$. For $\tau > 1$, $\langle\varepsilon_\theta\rangle$ is dominated by a balance between the production of $\langle\varepsilon_\theta\rangle$ arising from turbulent vortex stretching, and dissipation of $\langle\varepsilon_\theta\rangle$ by molecular processes, as first predicted by Corrsin (1953). However, further details bear noting. Firstly, when considering the relative magnitudes of the various terms for the different initial conditions, it is clear that the magnitudes of the terms for the IC_x condition are the largest, followed by those corresponding to the IC_z initial condition. Those corresponding to the IC_y initial condition are the smallest. Using the peak value of the molecular dissipation of $\langle\varepsilon_\theta\rangle$ (i.e. term (ix), light green line) as a reference, its value for IC_x is 4×10^{-5}, for IC_z is 2×10^{-5}, and for IC_y is 1×10^{-5}. Thus the larger values of all terms in the scalar field arising from the IC_x initial condition lead to the largest peaks of $\langle\varepsilon_\theta\rangle$, as well as the fastest decay rates of $\langle\varepsilon_\theta\rangle$, consistent with figure 4. Moreover, the converse holds for IC_y, which experiences the lowest peak value of $\langle\varepsilon_\theta\rangle$ and slowest decay rates. Secondly, one can observe in figure 5 that the two dominant terms (production of $\langle\varepsilon_\theta\rangle$ by turbulent vortex stretching and molec-

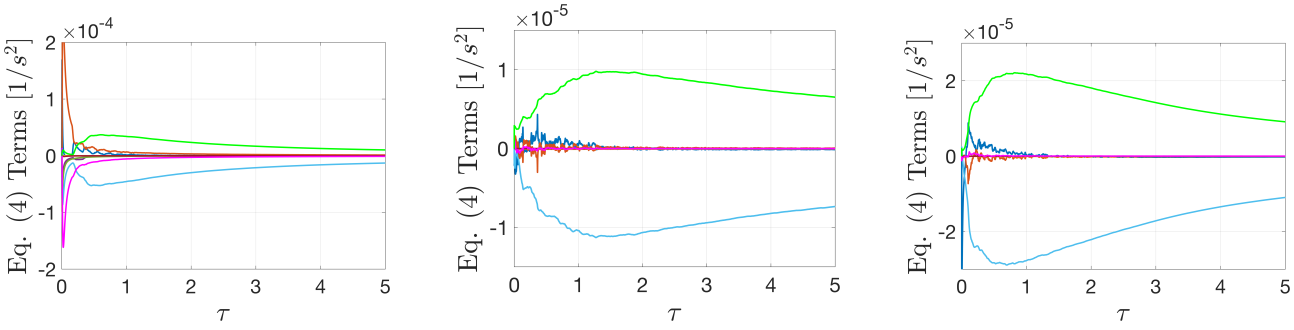

(a) IC_x (b) IC_y (c) IC_z

Figure 6: Evolution in time of the time-averages of all 9 terms in the scalar dissipation rate budget in which statistical moments ($\langle\cdot\rangle$) are assessed on the y-z plane at $x/L_x = 0.50$, i.e. $\frac{1}{\tau}\int_0^\tau Term\, d\tau'$, where all averages ($\langle\cdot\rangle$) in $Term$ are given by $\langle\cdot\rangle = \langle\cdot\rangle_{y,z}$.

ular dissipation of $\langle\varepsilon_\theta\rangle$) peak at later times for IC_y (at $\tau > 1$) than they do for the IC_x and IC_z cases (which peak at $\tau < 1$). This behaviour is also consistent with the evolutions of $\langle\varepsilon_\theta\rangle$ in figure 4, noted above.

We further investigate the budget of the scalar dissipation rate for the three initial conditions by plotting the time evolution of terms when spatially averaged over a single y-z plane in figure 6. Note that the plane over which the spatial averaging is performed in figure 6 is parallel to the interface between the "black" and "white" fluids in the IC_x initial condition, and located at the mid-plane of the channel in the x-direction (i.e. $x/L_x = 0.5$), i.e. the location of one of the two interfaces between the "black" and "white" fluids at $\tau = 0$ for IC_x. In figure 6, it is first worth noting the qualitative similarities of the evolutions of the terms in the $\langle\varepsilon_\theta\rangle$ budget for the IC_y and IC_z initial conditions. These two subfigures exhibit similar behaviours due to the absence of terms associated with spatial gradients of statistical moments in the directions of the averaging in the respective figures. We also note that analogous similarities are observed when reproducing the equivalent of figure 6, but spatial averaging in the other two (x-z and x-y) mid-planes (not shown). However, in contrast to figures 6(b) and 6(c), figure 6(a) is dominated at early times by mean-flow advection of $\langle\varepsilon_\theta\rangle$ and turbulent advection of $\langle\varepsilon_\theta\rangle$. This will be further discussed with respect to figure 7, which follows.

To investigate the evolution of the terms in the $\langle\varepsilon_\theta\rangle$ budget that are *not* subjected to such an artefact, we plot in figure 7 their evolution in time assessed on the mid-plane corresponding to the initial location of the interface for the three initial conditions. It reveals that figure 7(a), which corresponds to the IC_x initial condition, is significantly different from those corresponding to IC_y (7(b)) and IC_z (7(c)), which are quite similar. Whereas the dominant terms in figures 7(b) and 7(c) are the molecular dissipation of $\langle\varepsilon_\theta\rangle$, the production of $\langle\varepsilon_\theta\rangle$ by turbulent vortex stretching, production of $\langle\varepsilon_\theta\rangle$ by mean scalar gradients, the rate of change of $\langle\varepsilon_\theta\rangle$ with time, and turbulent advection of $\langle\varepsilon_\theta\rangle$, figure 7(a) is distinctly different. Of particular note is the importance played by mean-flow advection of $\langle\varepsilon_\theta\rangle$ at early times, which is dominant for $\tau < 0.2$, and balanced by turbulent advection of $\langle\varepsilon_\theta\rangle$. Given that fully developed turbulent channel flow must be unidirectional, the absence of the mean-flow advection term in the other directions is to be expected. However, the early dominance of this term is noteworthy. In this respect, consideration of the evolution in time of the interface(s) between the "black" and "white" fluids is beneficial. For the IC_y case, the $\langle\Theta\rangle = 0$ plane will not change in time and will be advected along the $y/h = 1$ plane as the flow evolves, but remaining at the same location as the initial interface. However, the evolution of the scalar field in time is quite different for IC_x. The interface remains "anchored" to the walls due to the no-slip condition, and is strongly stretched in the x-direction by the mean flow, while being stirred by the turbulence. Thus as the interface is advected downstream, it can "blow by" a given downstream location multiple times. This effect can be observed by the oscillations in the unsteady term (dark blue line), and to a lesser degree the mean flow advection terms (red line) in figure 7(a). It is worth noting that the period of the observed oscillation is indeed equal to half of the channel's "flow-through" time (i.e. $\frac{1}{2}\tau_{FT} \equiv \frac{1}{2}(L_x/\langle U\rangle_{y/h=1})u_\tau/h = 0.17$). With respect to IC_z, the $\langle\Theta\rangle = 0$ plane will be advected downstream the mid-plane of the channel ($z = 0.5L_z$), although its top and bottom edges will remain anchored to the walls of the channel, thus emulating aspects of both IC_x and IC_y.

Given that the results in figure 7 are all averages taken at the three midplanes of the channel, they are somewhat anomalous. For example, when averaging in the x- and z-directions at $y/h = 1$ (as is the case in figure 7(b)), there can be no contribution to $\langle\varepsilon_\theta\rangle$ arising from production by the mean velocity gradient because $\partial\langle U\rangle/\partial y = 0$ at that one location (and no other). Thus it bears investigating the budget of the scalar dissipation rate for the three initial conditions at non-mid-plane locations. To this end, the evolutions of the terms in the budget of the scalar dissipation rate are plotted for IC_x spatially averaged over an y-z plane located at $x/L_x = 0.25$ in figure 8(a), for IC_y spatially averaged over an x-z plane located at $y/h = 0.5$ in figure 8(b), and for IC_z spatially averaged over an x-y plane located at $z/L_z = 0.25$ in figure 8(c). The aforementioned periodic passing of the interface over the measurement plane for the IC_x case is even more prominent in figure 8(a). However, figures 8(b) and 8(c) also reveal another phenomenon that explains the slower evolutions of $\langle\varepsilon_\theta\rangle$ for the IC_y and IC_z cases. In these two non-mid-plane cases, one observes an initial period of "inactivity." The initial period in which the terms in the budget of $\langle\varepsilon_\theta\rangle$ are effectively zero results from the interface having not yet "reached" the measurement location. In these two cases, the interface can only travel laterally by the action of the turbulence, given that there is no mean velocity in the y- and z-directions. This phenomenon i) is not observed for the IC_x case, because the interface can be advected by the non-zero mean flow, and ii) further explains the slower evolutions of $\langle\varepsilon_\theta\rangle$ for the IC_y and IC_z cases, given that regions located increasingly far away from the interface experience a delay before they begin to mix. This latter effect therefore serves to retard the total mixing, because the interface surface is not normal to the mean velocity vector.

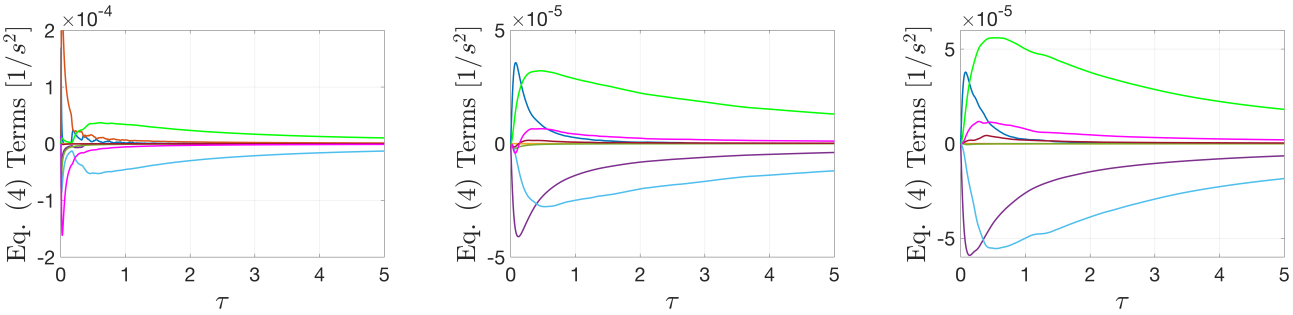

(a) IC_x (b) IC_y (c) IC_z

Figure 7: Evolution in time of the time-averages of all 9 terms in the scalar dissipation rate budget in which statistical moments ($\langle\cdot\rangle$) are assessed on the mid-plane corresponding to the initial location of the interface in the initial condition: $\frac{1}{\tau}\int_0^\tau Term\, d\tau'$. (a) IC_x with statistical moments evaluated over the y-z plane at $x/L_x = 0.50$, (b) IC_y with statistical moments evaluated over the x-z plane at $y/h = 1$, and (c) IC_z with statistical moments evaluated over the x-y plane at $z/L_z = 0.50$.

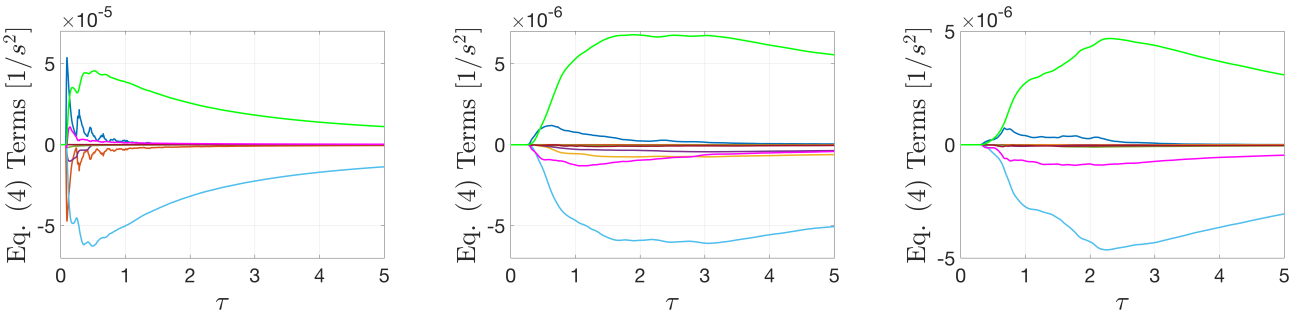

(a) IC_x (b) IC_y (c) IC_z

Figure 8: Evolution in time of the time-averages of all 9 terms in the scalar dissipation rate budget in which statistical moments ($\langle\cdot\rangle$) are assessed in planes parallel to the initial location of the interface in the initial condition, but *away from the mid-plane*: $\frac{1}{\tau}\int_0^\tau Term\, d\tau'$. (a) IC_x with statistical moments evaluated over the y-z plane at $x/L_x = 0.25$, (b) IC_y with statistical moments evaluated over the x-z plane at $y/h = 0.5$, and (c) IC_z with statistical moments evaluated over the x-y plane at $z/L_z = 0.25$.

CONCLUSIONS AND FUTURE WORK

In an attempt to better understand mixing within wall-bounded flows, with the ultimate goal of optimizing mixing processes, the present work has investigated the mixing of a scalar within a fully developed turbulent channel flow when subjected to three different initial conditions. A study of the temporal evolution of the terms in the scalar dissipation rate budget for the different initial conditions investigated why the IC_x case mixed most rapidly, and the IC_y case most slowly. It was found that the magnitude of the terms in the $\langle\varepsilon_\theta\rangle$ budget were consistent with both large values of $\langle\varepsilon_\theta\rangle$ and rapid decay rates of $\langle\varepsilon_\theta\rangle$. The stretching of the interface by the mean velocity field was also hypothesized to play an important role. To promote mixing in a wall-bounded flow, it is recommended that scalar interfaces be aligned normal to the mean velocity vector, to enhance the stretching of the interface. Whereas the general trends in the unmixedness and mix-norm were similar to those of $\langle\varepsilon_\theta\rangle$ for $\tau > 1$, future work should investigate their relationship during the initial phases of the mixing process.

REFERENCES

Corrsin, S. 1953 Remarks on turbulent heat transfer. *Proc. Iowa Thermodynamics Symposium, State University of Iowa, Iowa City,* pp. 5–30.

Danckwerts, P. V. 1952 The definition and measurement of some characteristics of mixtures. *Appl. Sci. Res.* **A3**, 279.

Dimotakis, P. E. & Miller, P.L. 1990 Some consequences of the boundedness of scalar fluctuations. *Phys. Fluids A* **2**, 1919.

Germaine, E., Mydlarski, L. & Cortelezzi, L. 2013 3DFLUX: A high-order fully three-dimensional flux integral solver for the scalar transport equation. *J. Compute. Phys.* **240**, 121.

Germaine, E., Mydlarski, L. & Cortelezzi, L. 2018 Persistence of local anisotropy of passive scalars in wall-bounded flows. *Phys. Rev. Fluids* **3(1)**, 014606.

Gibson, J. F. 2010 Channelflow: A spectral Navier-Stokes simulator in C++, licensed under the GNU GPL, `http://channelflow.org/`. *Tech. Rep.*. University of New Hampshire.

Gibson, J. F., Halcrow, J. & Cvitanović, P. 2008 Visualizing the geometry of state space in plane Couette flow. *J. Fluid Mech.* **611**, 107–130.

Gubanov, O. & Cortelezzi, L. 2009 Sensitivity of mixing optimization to the geometry of the initial scalar field. In *Analysis and Control of Mixing with an Application to Micro and Macro Flow Processes* (ed. L. Cortelezzi & I. Mezić), pp. 369–405. Vienna: Springer.

Li, S., Jaroszynski, S., Pearse, S., Orf, L. & Clyne, J. 2019 VAPOR: A visualization package tailored to analyze simulation data in earth system science. *Atmosphere* **10** (9).

Mathew, G., Mezić, I. & Petzold, L. 2005 A multiscale measure for mixing. *Physica D* **211**, 23.